

Magnetically Guided Liquid Metal Divertor (MAGLIMD) with Resilience to Disruptions and ELMs

Michiya SHIMADA and Kenji TOBITA

*National Institutes for Quantum and Radiological Science and Technology,
Fusion Energy Research and Development Directorate,
Rokkasho Fusion Institute,
2-166 Omotedate, Obuchi, Rokkasho, Kamikita, Aomori 039-3212, Japan*

(Received 20 June 2019 / Accepted 23 February 2020)

An innovative concept for power and particle removal from the divertor is proposed. This scheme takes full advantage of both liquid metal convection and conduction to remove heat from the divertor, which is the most difficult issue for fusion reactor design. We propose that a liquid metal (LM) should replace the solid divertor plates on the bottom of the vacuum vessel. The LM is continuously supplied from openings located at the inner separatrix strike point on the floor of the LM container on the bottom of the vacuum vessel, and exhausted from openings located at the outer separatrix strike point on the floor of the LM container. The LM flow is guided along the field line to reduce MHD drag. In the event of a disruption, the current induced in the LM during the current quench is in the same direction of the plasma current. The induced LM current would either attract the plasma toward the LM divertor (leading to a benign Vertical Displacement Event), or force the LM toward the core plasma, providing automatic disruption mitigation, not requiring a learning process. The use of liquid tin instead of liquid lithium would provide greater stability against Rayleigh-Taylor and Kelvin-Helmholtz instabilities in quiescent plasmas.

© 2020 The Japan Society of Plasma Science and Nuclear Fusion Research

Keywords: fusion reactor, divertor, liquid metal, plasma facing component, power exhaust, particle control, disruption

DOI: 10.1585/pfr.15.1401011

1. Introduction

The removal of extremely high heat loads on the divertor poses the most challenging issue for DEMO designs, and unmitigated edge localised modes (ELMs) and disruptions will cause melting and subsequent deformation of tungsten target surfaces, raising a very serious concern for ITER and DEMO. The EFDA Report [1] indicates that “[a] solution for the heat exhaust in the fusion power plant is needed. A reliable solution to the problem of heat exhaust is probably the main challenge towards the realisation of magnetic confinement fusion. The risk exists that the baseline strategy pursued in ITER cannot be extrapolated to a fusion power plant. Hence, in parallel to the programme in support of the baseline strategy, an aggressive programme on alternative solutions for the divertor is necessary.” The report by the Japanese Joint-Core Team for the Establishment of Technology Bases Required for the Development of a Fusion DEMO Reactor [2] also points out that “[with] regard to the concern with the divertor heat load, this cannot be solved in a simple way because there are major gaps between required conditions and present technologies”.

Presently, the standard material for the divertor of ITER [3] and DEMO [4] is tungsten, mainly due to its high melting point and low tritium retention. However, tungsten

targets may melt as a result of the thermal quenches associated with several hundred unmitigated disruptions/VDEs and ELMs, even in the H/He stage of ITER [3]. A recent survey [5] points out that the complete suppression of these transients, even in DEMO, would be extremely difficult. Other potential issues for tungsten include tritium retention in deep traps produced by neutron damage, serious surface damage and erosion caused by high cycle pulse heat loads well below the melting threshold, surface modification with He bubbles, nano-fibers, He holes, cracking due to increase in the ductile-to-brittle transition temperature (DBTT), radiation hardening, void swelling, etc. [5]. A strong effort for the development of alternative materials is thus called for.

An actively-convected liquid metal divertor (ACLMD) was proposed to provide a solution to these two problems [6]. The ACLMD employs a liquid metal (LM) in place of solid divertor targets. In the original scheme, toroidal electrodes embedded in the LM enable active convection induced by the $\mathbf{J} \times \mathbf{B}$ force, where \mathbf{J} is the current in the LM and \mathbf{B} is the magnetic field. The active convection spreads the heat from the plasma deposited on narrow zones to a large volume/surface, significantly facilitating heat removal. After ELMs and disruptions, the LM will quickly recover a flat surface and

author's e-mail: michiya.shimada@gmail.com

its heat removal capability. This stands in striking contrast with a conventional tungsten target, which would require replacement after unmitigated disruptions and ELMs because heat handling could seriously deteriorate due to surface deformation after melting and re-solidification. Proof-of-principle (PoP) experiments for the ACLMD were carried out in NIFS, demonstrating that the ACLMD also provides a means to pump particles in steady state [7].

This paper proposes an innovative concept of power and particle control. The LM flow guided along the field line, which reduces MHD drag, is the key to strong convection. The need of electrodes for LM motion is also eliminated.

Furthermore, implementation of a LM divertor could enhance the resilience of a tokamak reactor to disruptions and ELMs. In the event of a disruption, the current induced in the LM during the current quench is in the same direction of the plasma current, would either attract the plasma toward the LM divertor (resulting in a benign Vertical Displacement Event), or force the LM toward the core plasma, enabling automatic disruption mitigation. The eddy currents induced in the LM during an ELM and the consequent LM ejection can be substantially reduced by electrically separating the inner and outer divertor channels. If this concept works, it could greatly mitigate the divertor heat handling problem and problems associated with disruptions and ELMs, facilitating the design, construction, operation and maintenance of future reactors.

Although comparison of liquid metals is beyond the scope of this paper, tin is a good candidate for the liquid metal material for a divertor, due to its low melting temperature, low vapour pressure, low toxicity and low chemical activity. Other characteristics of tin are discussed by Miyazawa [8].

2. Liquid Metal Flow Rate Required to Remove Heat

First, let us discuss the liquid metal flow rate required to remove heat from the divertor. We estimate the LM flow rate required to remove power P (W) with the following formula, assuming liquid tin with mass density ρ (kg/m³), specific heat C (J/kg/deg), flow rate Γ (m³/s), temperature of supplied tin T_{in} (degree C), and temperature of exhausted tin T_{out} (degree C):

$$\Gamma = \frac{P}{\rho C (T_{out} - T_{in})},$$

with $P = 400$ MW, $\rho = 7 \times 10^3$ kg/m³, $C = 228.4$ J/kg/deg, $T_{out} = 400^\circ\text{C}$, and $T_{in} = 300^\circ\text{C}$, we obtain $\Gamma = 2.5$ m³/s.

The power P_{drive} required to drive the LM flow Γ against the gravitational force is given by:

$$P_{drive} = \rho g h \Gamma \sim 2 \text{ MW},$$

for $g = 9.8$ m/s² (gravitational acceleration) and $h = 10$ m (height of the divertor LM surface measured from the electromagnetic pump (EMP)). This power is negligible com-

pared with the power the LM divertor will handle.

The flow speed $v_{//}$ along the field line is estimated to be:

$$v_{//} = \frac{\Gamma}{2\pi R w \theta} = \frac{2.5}{2\pi \cdot 8.5 \cdot 0.2 \cdot 0.05} = 5 \text{ m/s},$$

using a major radius R of 8.5 m [4], a tube width w of 0.2 m, and a field line pitch θ ($= B_p/B_t$, where B_p and B_t are the poloidal and toroidal magnetic field, respectively) of 0.05 are assumed. It is also assumed that the inlets and outlets are installed at intervals of h/θ , where h is the height of the inlets/outlets such that all the in-flow and out-flow around the toroidal direction (θ) are supplied and exhausted by the inlets/outlets, which are discussed further in the next session.

3. Concept of MAGLIMD

This scheme is based upon a very fundamental principle: liquid metal is mobile along the field line. In the simplest scheme (Figs. 1 - 3), all that is needed are a toroidally-continuous LM container, outlet tubes of LM with openings located near the separatrix strike point on the outboard bottom of the LM container, as well as LM inlet tubes with openings located near the separatrix strike point on the inboard bottom of the LM container. The flow from the inlet to the LM surface is driven by an EMP. The flow in the private flux region, having a component across the field line, is driven by a centrifugal force (present in the moving frame) or a pressure gradient, which will be discussed in the next section. The flow from the LM surface to the outlet is driven by the gravitational force. This scheme is much more compact than the original Slim-CS divertor [9] and ACLMD [6].

Since the LM flow along the field line does not suffer from MHD drag, the LM volume that is directly connected to the outlet along the field line will be exhausted at that location, whereas the LM in the neighbouring volume will flow in. The LM in the volume that is directly connected to the inlet along the field line will flow out from that location. Since the LM connected to the outlet and the LM connected to the inlet flow in the same toroidal direction, the whole LM will rotate toroidally due to viscosity. Consequently, the uniformity of LM characteristics (temperature and particle inventory) toroidally will be improved, despite the fact that the openings for LM supply and exhaust can be provided only at discrete locations in the toroidal direction.

If necessary, further enhancement of toroidal uniformity is possible. In a fusion reactor, where the divertor configuration is fixed and the field line forms a grazing angle with respect to the LM surface, inlet/outlet openings can be arranged in such a way that all the in-flow and out-flow around the toroidal direction are supplied and exhausted by the inlets/outlets, although the openings are installed at only discrete locations in the toroidal direction (Fig. 4).

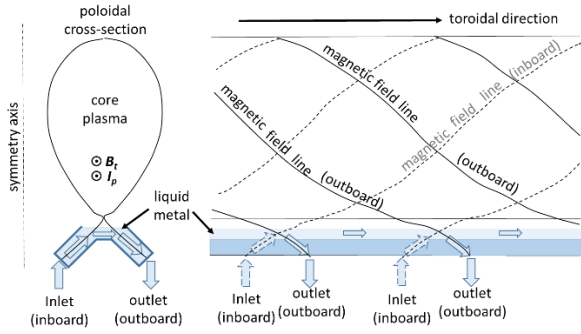


Fig. 1 Poloidal cross-section of a tokamak with MAGLIMD and its side view. The solid lines of the side view indicate magnetic field lines running on the outboard separatrix surface and the broken lines magnetic field lines running on the inboard separatrix surface.

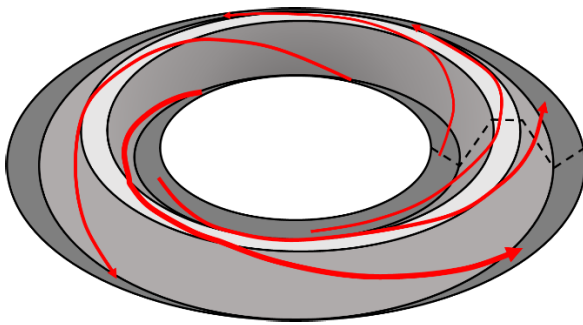


Fig. 2 Bird's eye view of MAGLIMD and the LM flow.

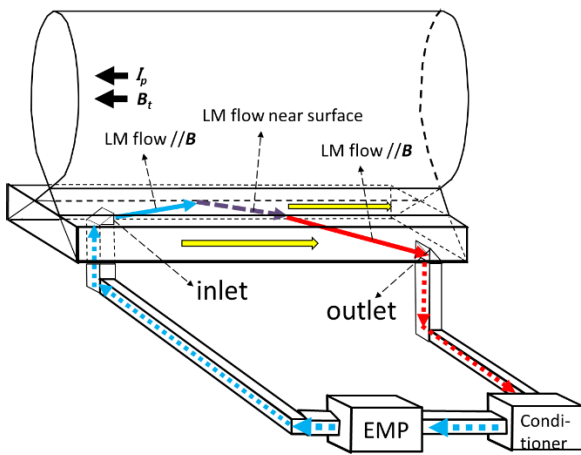


Fig. 3 Schematic of MAGLIMD. The solid arrows indicate LM flows along the field line. LM is injected from the inlets installed on the separatrix strike point on the inboard floor of the LM container, driven by an electromagnetic pump (EMP). The injected LM flows along the field line up to the LM surface. The LM is exhausted from the outlets installed on the separatrix strike point on the outboard floor of the LM container. The LM flows along the field line up to the outlet. The dotted arrows indicate flows across the field line. Insulation of the container wall and inlet/outlet tubes significantly reduces MHD drag. The arrows within the LM container indicate the direction of the LM toroidal flow.

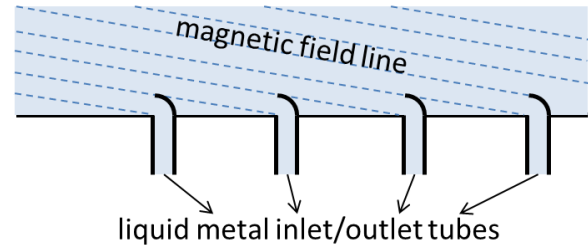


Fig. 4 In a fusion reactor, where the divertor configuration is fixed and the field line in the LM divertor forms a grazing angle with respect to the surface, inlet/outlet openings can be arranged in such way that all the in-flow and out-flow around the toroidal direction are supplied and exhausted by the inlets/outlets despite the openings being installed at only discrete locations in the toroidal direction.

In the simplest configuration, the LM flow is driven if there is an LM inlet and an outlet that are both on the same field line (Fig. 5 (a)). If the field is perpendicular to the flow velocity \mathbf{v} , a $\mathbf{v} \times \mathbf{B}$ electromotive force will be induced. If the container is conductive, the $\mathbf{j} \times \mathbf{B}$ force would drag the flow (i.e., via MHD drag). However, if the container or the inner wall of the container is insulated, the MHD drag would be significantly reduced (Fig. 5 (b)).

Let us discuss the case of an LM container that is toroidally continuous with its insulated inner wall and the magnetic field \mathbf{B} oblique to the LM surface in the toroidal direction. If there is a radial flow velocity \mathbf{v} , the toroidal current \mathbf{j} should be considered in the force balance (Fig. 5 (c)). With the LM velocity \mathbf{v} in the radial direction, the $\mathbf{v} \times \mathbf{B}$ electromotive force drives a current \mathbf{j} in the toroidal direction if the magnetic field \mathbf{B} is oblique to the LM surface in the toroidal direction (Fig. 5 (d)). The toroidal current \mathbf{j} and the magnetic field \mathbf{B} oblique to the LM surface will lead to the $\mathbf{j} \times \mathbf{B}$ drag force.

However, a simple estimate of the MHD drag (W_{drag}) indicates that due to geometry (i.e., the grazing angle between the field line and the LM surface) and the centrifugal force, the MHD drag is acceptable. Figure 6 (a) shows a plan view for the divertor configuration in Fig. 1. The toroidal flow component in the private flux region is removed for simplicity. The flow (v_{surface}) in the private flux region involves motion across the field line, which induces $\mathbf{v} \times \mathbf{B}$ force that is nearly vertical, particularly near the LM surface. The current only flows in the toroidal direction, and the field line is nearly horizontal (Figs. 6 (b) and (c)). The toroidal current is driven by the toroidal component of force due to the perpendicular electric field (\mathbf{E}_{\perp}), which is almost vertical (Fig. 6 (d)). The MHD drag (W_{drag}) is therefore

$$\begin{aligned}
 W_{\text{drag}} &= \mathbf{j}_{\perp} \mathbf{B} \cdot 2\delta \\
 &= \theta \mathbf{j}_{\text{toroidal}} \mathbf{B} \cdot 2\delta \\
 &= \theta \sigma \mathbf{E}_{\text{toroidal}} \mathbf{B} \cdot 2\delta \\
 &= \theta^2 \sigma \mathbf{E}_{\perp} \mathbf{B} \cdot 2\delta \\
 &= \theta^2 \sigma v_{\perp} B^2 \cdot 2\delta
 \end{aligned}$$

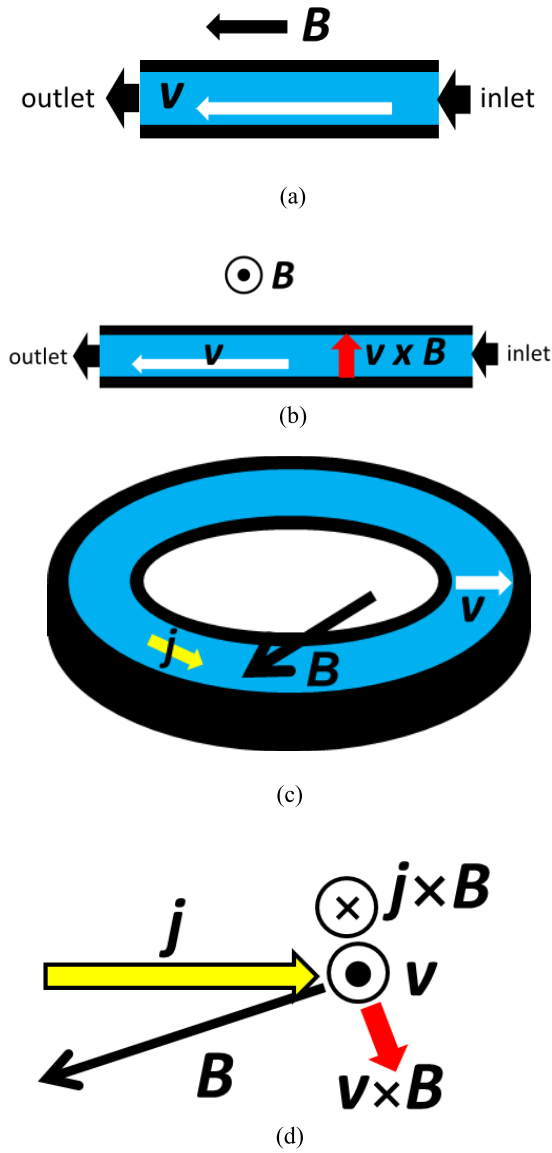


Fig. 5 (a) LM flow parallel to B and (b) LM flow perpendicular to B associated with the $v \times B$ electromotive force; use of an electrical conductor for the inner wall would lead to a drag on the LM flow (i.e., MHD drag); insulation of the inner wall would significantly reduce the MHD drag. (c) LM in a toroidal container, where the field line lies obliquely to the surface. If the LM has velocity v across the field, the toroidal current j should be considered in the force balance. (d) With the LM speed v in the radial direction (Fig. 5 (c)), the $v \times B$ electromotive force drives a current j in the toroidal direction if the magnetic field B is oblique to the LM surface in the toroidal direction. The toroidal current j and the magnetic field B oblique to the LM surface will result in the $j \times B$ drag force.

$$= \theta^3 \sigma v_{//} B^2 \cdot 2\delta,$$

or

$$\begin{aligned} W_{\text{drag}} &\sim (0.05)^3 \cdot 2 \times 10^6 \cdot 5 \cdot 6^2 \cdot 0.04 \\ &\sim 1800 \text{ Pa} \\ &\sim 0.018 \text{ atm.} \end{aligned}$$

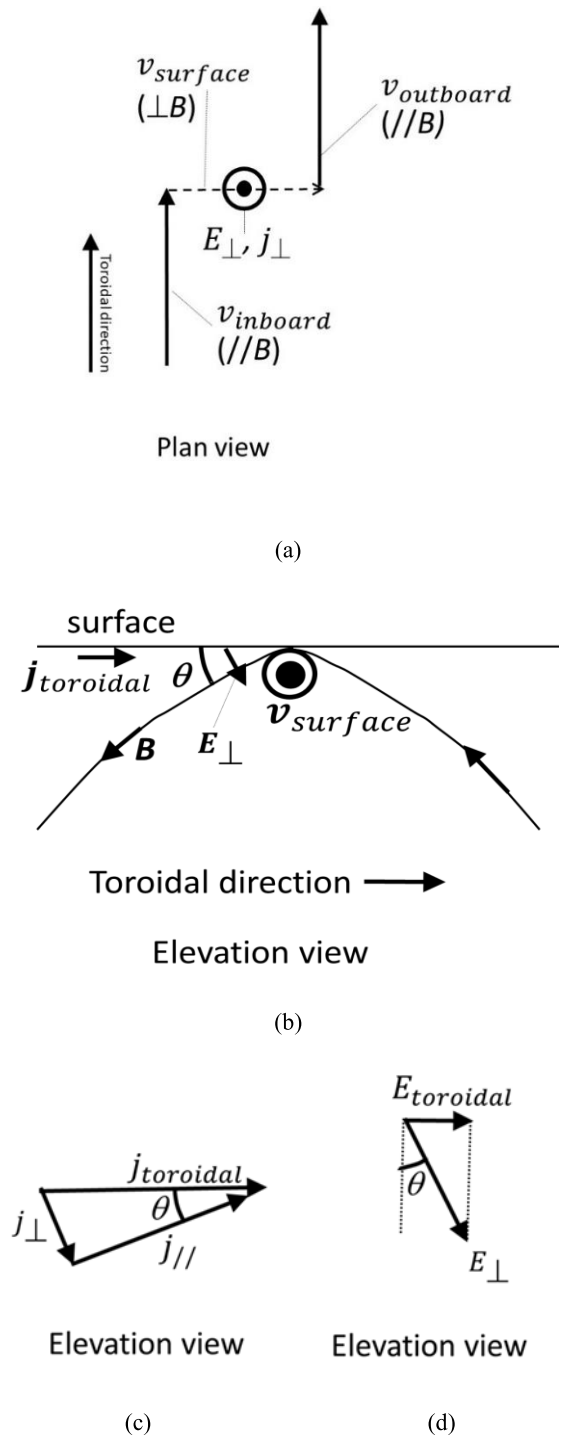


Fig. 6 (a) Plan view of Fig. 1 showing the direction of the LM flow. The toroidal component of the flow along the field line in the private flux region is removed for simplicity. (b) Elevation view of Fig. 1. (c) Elevation view of toroidal current j_{toroidal} , with its major component $j_{//}$ (parallel to B) and a small component j_{\perp} (perpendicular to B). (d) Elevation view of the electric field E_{\perp} (which enables a $v \times B$ force to be induced), with its small toroidal component (E_{toroidal}) driving the toroidal current (j_{toroidal}).

Here, j_{\perp} is the current density perpendicular to the magnetic field $B \sim 6 \text{ T}$, $\delta \sim 0.02 \text{ m}$ is the cross-field length (Fig. 7), $\theta \sim 0.05$ radian is the angle between the magnetic

field and the liquid surface, j_{toroidal} is the toroidal current density, $\sigma \sim 2 \times 10^6$ S/m is the electrical conductivity of liquid tin just above the melting temperature, E_{toroidal} is the toroidal electric field, and E_{\perp} is the electric field perpendicular to the magnetic field. It is also assumed that $v_{\perp} \sim v_{\parallel}/\theta$. This estimate suggests that a step ~ 2.6 cm in height on the LM surface would make a pressure gradient across the field line, which could balance the MHD drag.

Furthermore, the work done by the centrifugal force W_{cf} (as present in the moving frame) can be made stronger than the MHD drag.

$$W_{cf} = (\rho v_{\parallel}^2 / R) \cdot \Delta.$$

Where $\Delta \sim 0.2$ m is the radial distance of the private region where the centrifugal force is active (Fig. 7).

$$\begin{aligned} \frac{W_{cf}}{W_{drag}} &= \frac{\rho v_{\parallel} \Delta / R}{\sigma \theta^3 B^2 2\delta} \\ &\sim \frac{7 \times 10^3 \times 5 \times 0.2 / 8.5}{2 \times 10^6 \times 0.05^3 \times 6^2 \times 2 \times 0.02} \sim 2. \end{aligned}$$

The MHD drag on the LM flowing in the duct perpendicular to the magnetic field is analyzed with a formula derived by Shercliff [10]. The Hartmann number H is given by:

$$H = Ba(\sigma/\mu)^{1/2},$$

where B is the magnetic field (T), a is the half size of the duct, σ is the electrical conductivity of the LM, and μ is the viscosity of the LM.

The MHD drag is given by:

$$\frac{\partial p}{\partial z} \sim -\frac{v}{a^2} H \mu,$$

where p is the pressure of the LM, z is the distance along the duct, and v is the LM velocity. The wall contacting the LM is insulated.

For $B = 6$ T, $a = 0.1$ m, $\sigma = 2 \times 10^6$ S/m, $\mu = 1.85 \times 10^{-3}$ Pa·s [11] and $v = 5$ m/s, we obtain

$$H \sim 2.0 \times 10^4,$$

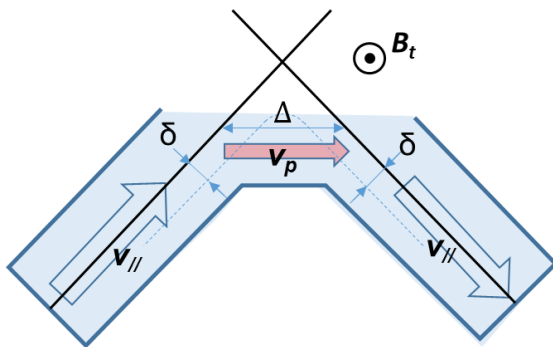


Fig. 7 Various parameters for the MAGLIMD.

$$\left| \frac{\partial p}{\partial z} \right| \sim 2 \times 10^4 \text{ Pa/m.}$$

With a duct length of 10 m running perpendicular to the magnetic field, the MHD drag is $\sim 2 \times 10^5$ Pa, which is within an acceptable range.

4. Start-Up and Shutdown

At the discharge start-up and shutdown, a toroidal current can be induced in the LM. Consideration of the electromagnetic force on the LM is required.

4.1 Start-up in the limiter configuration

At the discharge start-up in a limiter configuration, the LM would be ejected if the $j \times B$ force exceeds the gravitational force (Fig. 8 (a)).

$$J_{\text{toroidal}} B_p > \rho g, \text{ where } j_{\text{toroidal}} \sim \sigma E,$$

E is the toroidal electric field.

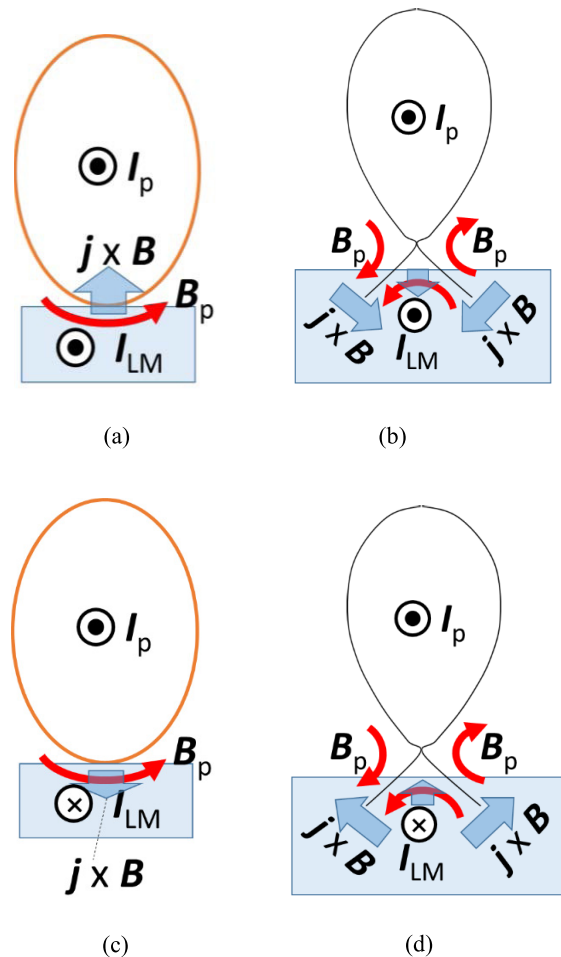


Fig. 8 (a) Discharge start-up in the limiter configuration (b) Current induced in LM and the resultant $j \times B$ force at the discharge start-up in the divertor configuration. (c) Discharge shutdown in the limiter configuration. (d) Current induced in the LM and the resultant $j \times B$ force at discharge shutdown in the divertor configuration.

$$E > \frac{\rho g}{\sigma B_{p_p}},$$

$$E > \frac{7 \times 10^3 \cdot 9.8}{2 \times 10^6 \cdot 0.2} = 0.17 \text{ V/m}.$$

$B_p \sim 0.2 \text{ T}$ is assumed. At the discharge start-up, the minimum toroidal electric field is estimated to be 0.3 V/m [12]. This suggests that the divertor might have to be empty of LM at the start-up, and the LM should be supplied after the electric field is below this value.

4.2 Discharge start-up in the divertor configuration

At the discharge start-up in a divertor configuration, a current will be induced in the LM in the same direction as the plasma current, but the LM would not be ejected toward the core (Fig. 8 (b)).

The induced LM current (I_{LM}) and the poloidal field from it would *not* disturb plasma operations. The magnitude of I_{LM} can be estimated as follows.

$$I_{LM} \sim \frac{\sigma V_l}{2\pi R} \cdot A_{LM},$$

$$I_{LM} \sim \frac{2 \times 10^6 \cdot 1}{2\pi \cdot 8.5} \cdot 0.1 \sim 4 \text{ kA}.$$

Note that the typical poloidal coil current of a reactor is 10 MA-turn . A one-turn loop voltage V_l of 1 V and a poloidal cross sectional area of the LM container A_{LM} of 0.1 m^2 (e.g., 0.5 m wide and 0.2 m deep) are assumed.

4.3 Discharge shutdown in the limiter configuration

At the discharge shutdown in the limiter configuration, a current is induced in the LM in the direction opposite to the plasma current. The LM will not be ejected in this case (Fig. 8 (c)).

4.4 Discharge shutdown in the divertor configuration

At the discharge shutdown in the divertor configuration, current will be induced in the LM in the direction opposite to the plasma current. The LM would not be ejected toward the core if the plasma current ramp down rate is sufficiently slow, and the toroidal electric field does not exceed the level discussed in Sec. 4.2 (Fig. 8 (d)).

5. Rayleigh-Taylor and Kelvin-Helmholtz Instabilities

5.1 Theoretical background

The free surface instability of liquid metal was analysed by Hassanein [13], Jaworski [14] and Fifiis [15].

The dispersion relation includes the determinant which is proportional to:

$$D = -\rho g + (\mathbf{j} \times \mathbf{B}) \cdot \mathbf{n} - \gamma k^2 + \rho_p v_p^2 k.$$

$D > 0$ means that the mode is unstable, and $D < 0$ indicates stability. k is the wavenumber normal to \mathbf{B} , which corresponds to the direction of greatest instability. The first term is gravitational force which is stabilising, and the second term is related to the electromagnetic force which is stabilising or de-stabilising depending on the sign of the vector product; the current density \mathbf{j} originates from the scrape-off layer (SOL) plasma and \mathbf{n} is the unit vector in the upward vertical direction. The third term represents the surface tension which is stabilising, and the last term the driving term for the Kelvin-Helmholtz instability due to the plasma mass flow and is destabilising; ρ_p and v_p are the mass density and flow velocity of the plasma. The equation can be rewritten with the last term reformulated by using the Bohm sheath condition:

$$D = -\rho g + (\mathbf{j} \times \mathbf{B}) \cdot \mathbf{n} - \gamma k^2 + p_p k.$$

Here p_p is the total plasma pressure at the sheath.

5.2 SOL current

The SOL current has been measured in many tokamaks during the quiescent phase of plasmas [16–18] and during ELMs [19–23]. The measured currents were largely consistent with the thermoelectric current theory [24,25] or the extension of the theory to electron pressure imbalance [26], which predicts that the SOL current flows from the higher T_e side to the lower T_e side. This corresponds usually to the SOL current flowing from outboard to inboard during the quiescent phase, and from inboard to outboard during ELMs for negative \mathbf{B} in the counter-clockwise direction, with the ion- $\nabla \mathbf{B}$ drift pointing downwards. The resultant electromagnetic force in the LM is stabilising during the quiescent phase and de-stabilising during ELMs (Fig. 9). In JT-60U, however, the sign of the SOL current was reversed when the divertor became detached or a MARFE developed at the X-point [18]. In JT-60U and

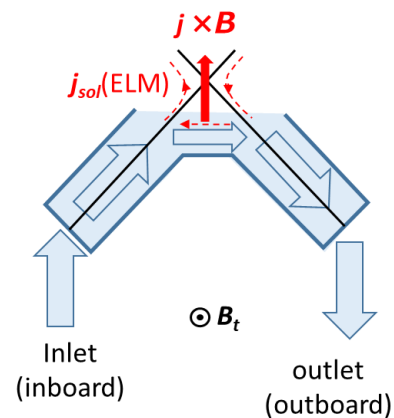


Fig. 9 The broken lines indicate ELM currents in the SOL and LM, which flow along \mathbf{B} in the plasma and across \mathbf{B} in the LM. The solid line shows the resultant electromagnetic force, ejecting the LM into the core.

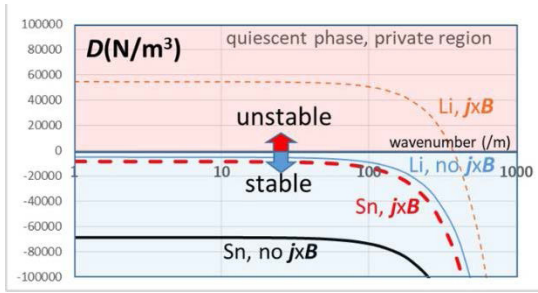


Fig. 10 Stability diagram for Li and Sn during the quiescent phase in the private flux region.

JET, SOL currents parallel to B were up to 2×10^5 A/m². In JET [19] and TCV [20], SOL currents parallel to B up to 1×10^6 A/m² were measured during ELMs. Jaworski [23] measured SOL currents $\sim 1 \times 10^4$ A/m² during quiescent phases and $\sim 1 \times 10^5$ A/m² during ELMs in NSTX, using probes installed flush to the divertor PFC surfaces. Assuming pitch angles in the range of 0.05 - 0.1 radians, the results from NSTX, JT-60U, JET and TCV are consistent with each other.

5.3 Private flux region

In the private flux region, i.e., the area between the inner and outer channels, there is no plasma. This eliminates the effect of the sheath plasma pressure p_p , so that the equation for D can be simplified:

$$D = -\rho g + (j \times B) \cdot n - \gamma k^2.$$

During the quiescent phase, if the electromagnetic force is pointing downward, the free surface in the private flux region is stable. If the electromagnetic force points upward, the free surface would be unstable for the case of lithium, but stable for the case of tin (Fig. 10), due to the higher mass of tin. Here, a poloidal current of 1×10^4 A/m², toroidal field of 6 T, gravitational acceleration of 9.8 m/s², lithium mass density of 0.512×10^3 kg m⁻³, lithium surface tension of 0.4 N/m [27], tin mass density of 6.99×10^3 kg m⁻³, and tin surface tension of 0.5 N/m [28, 29] are used.

A free surface of lithium can be stable during the quiescent phase at high wavenumbers (e.g., 10^3 m⁻¹). That is the motivation for using a capillary pore structure (CPS) with sub-mm pore dimensions [30], but this makes it difficult to rely on heat removal by convection. In contrast, a free surface of tin is stable during the quiescent phase due to its heavy mass, eliminating the flow constraints of the CPS and opening up the possibility of efficient heat removal with convection.

During ELMs, SOL currents are enhanced by an order of magnitude in comparison with the quiescent phase, which makes the free surface unstable even for the case of tin. Separating the two divertor channels and eliminating

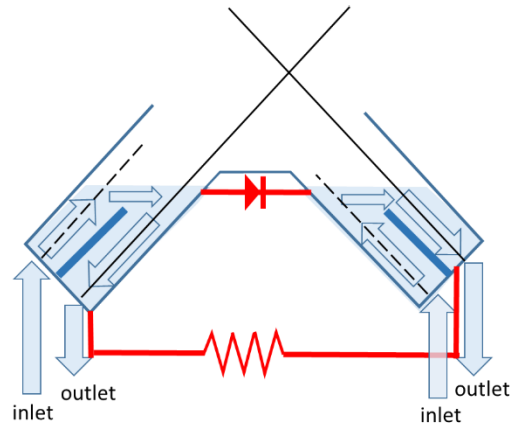
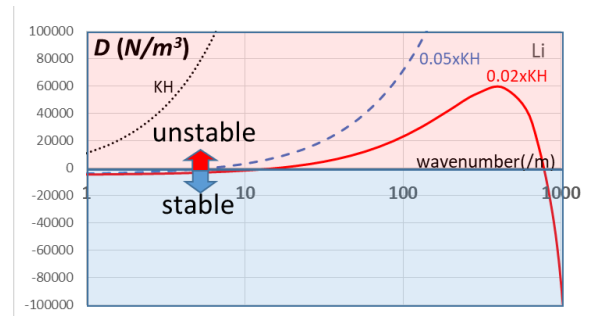
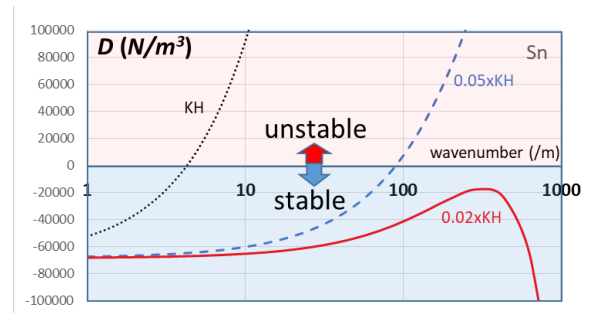


Fig. 11 MAGLIMD with two divertor channels separated electrically.



(a)



(b)

Fig. 12 (a) Kelvin-Helmholtz stability diagram of lithium surface. (b) Kelvin-Helmholtz stability diagram of tin surface.

the current flowing radially inward in the private flux region should significantly reduce the $j \times B$ force, and could enhance the stability of the free surface (Fig. 11). A diode is an option for controlling the current flow that might also improve the stability, provided that the $j \times B$ force is pointing downward.

5.4 LM surface in contact with the plasma

With the assumption that the Rayleigh-Taylor instability can be suppressed by separating the two divertor

channels (Fig. 11), the Kelvin-Helmholtz stability was examined. The parameters assumed for the plasma hitting the LM during an ELM were $n_e = 1 \times 10^{21} \text{ m}^{-3}$ and $T_e = 100 \text{ eV}$. Even with significant mitigation (e.g., a reduction by a factor of 50 in the pressure), a lithium surface is unstable over a wide range of wavelengths (Fig. 12 (a)). The tin surface is stable assuming a mitigation of a factor of 50 (Fig. 12 (b)), indicating the need of ELM mitigation methods, which have been under development for many years.

One should note here that the consequence of unmitigated ELMs is more serious for solid tungsten targets compared to LM targets. The ELMs will cause serious damage to the surface of tungsten targets, which would then have to be replaced. In the case of LM divertors, the surface flatness will be recovered quickly.

6. Prompt Redeposition at ELMs

The prompt redeposition of tungsten (W) is a particularly large effect with ITER ELMs, because of the high plasma density ($> 1 \times 10^{21} \text{ m}^{-3}$) and high electron temperature ($> 100 \text{ eV}$) near the divertor targets [31]. The formula for the fraction of non-redeposition $f_{non-reddep}$ [32] is given by:

$$f_{non-reddep} = \frac{p^2}{1 + p^2}, \quad p = \tau_{ion} \omega_{gyro} = \lambda_{ion} / \rho W_{max}.$$

When ELMs occur, $p \ll 1$, and $f_{non-reddep} \sim p^2 \ll 1$. The electric field in the magnetic pre-sheath (MPS) prevents the W ions from entering the main plasma beyond the MPS [31]. For the case of tin (Sn) under ELM conditions, $p \sim 0.01$ is estimated with ionization cross-section formulated in [33], indicating that similar to W, there is almost complete prompt redeposition of tin.

7. Disruptions

This section is focused on the discussion of what is expected to occur with the LM divertor during disruptions. A possible scheme to mitigate disruptions at an early stage of current quench (CQ) is also discussed.

7.1 Thermal quench

At the thermal quench (TQ), a large fraction of plasma energy W_{TQ} is expelled from the core and deposited onto the LM divertor in a short time Δt_{TQ} . The analysis of the consequence of the TQ, including vapour shielding, is beyond the scope of this paper. As experimentally observed [34, 35] and numerically predicted [36] for tungsten PFCs, however, a significant ingress of LM is expected into the core through “splashes” and cool the plasma. These splashes may result in radiative dissipation of the remaining thermal and magnetic energy and could provide disruption mitigation.

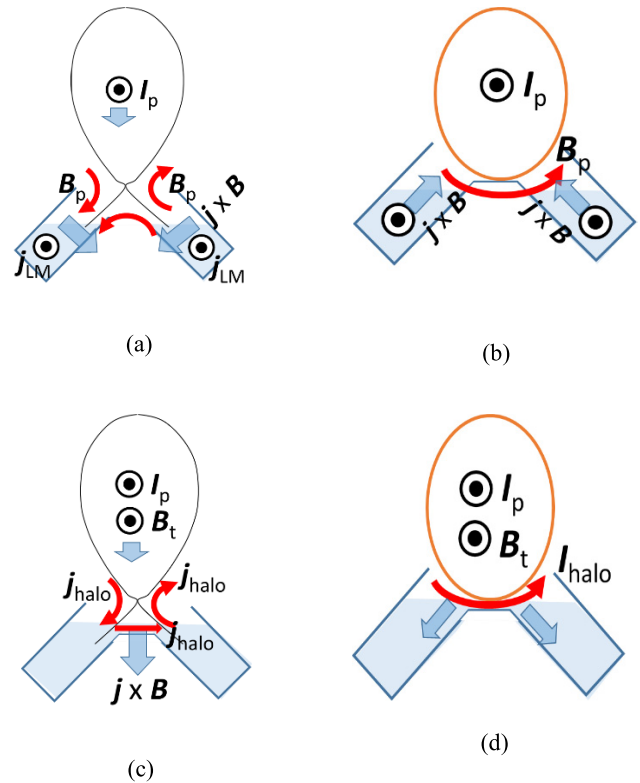


Fig. 13 (a) The toroidal currents induced in the LM, the poloidal magnetic field, and the electromagnetic force on the LM during the current quench in the divertor configuration. (b) The toroidal currents induced in the LM, the poloidal magnetic field, and the electromagnetic force on the LM during the current quench in the limiter configuration. (c) Halo currents in the divertor configuration. (d) Halo currents in the limiter configuration.

7.2 Current quench

At the current quench (CQ) of a disruption in a divertor configuration, a current will be induced in the LM in the same direction as the plasma current. Since the direction of the $j \times B$ force is facing away from the core (Fig. 13 (a)), the LM would not be ejected toward the core. The core plasma, however, would be attracted toward the divertor and result in a benign vertical displacement event (VDE), which will eventually result in a limiter configuration.

When the VDE leads to a limiter configuration, the $j \times B$ force due to the toroidal current induced in LM and the poloidal field will eject the LM into the core, resulting in *automatic disruption mitigation* (Fig. 13 (b)). The $j \times B$ force during the current quench would be much stronger than the gravitational force.

Since the vertical speed of the VDE is slow ($\sim 0.5 \text{ s}$), the height of the LM can be increased so that the top of the dome will be protected. The level of the liquid metal surface can be increased at a rate of $dh/dt \sim f/(2\pi R w) \sim 2.5/(2\pi \cdot 8.5 \cdot 0.5) \sim 0.1 \text{ m/s}$, suggesting that the top of the dome might be wetted by the LM in time to protect it against direct contact with the core plasma.

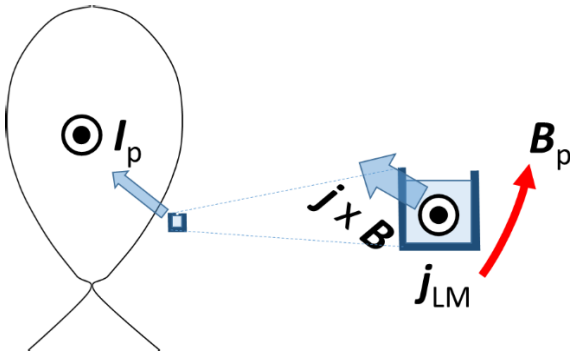


Fig. 14 Automatic disruption mitigator. A toroidally continuous tube, with its top open, is filled with LM. At the CQ, a toroidal current will be induced in the LM in the same direction as the plasma current. The Lorentz force will eject the liquid toward the core, which will result in radiative dissipation of the remaining plasma and magnetic energy.

The $j \times B$ force due to halo currents and the toroidal field does not eject the LM toward the core (Figs. 13 (c) and (d)).

7.3 Automatic disruption mitigator

The discussion in the previous subsections suggests that aside from possible splashes during the TQ, the current quench and halo current processes do not eject LM toward the core, unless the discharge is limited on the bottom. In case a more substantial scheme for automatic disruption mitigation is needed, the following arrangement could be useful.

A toroidally-continuous tube, installed on the lower midplane with its top open, is filled with LM (Fig. 14). At the current quench (CQ) of a disruption, a current will be induced in the LM in the direction of the plasma current. The resulting $j \times B$ force will eject the LM toward the core, providing automatic disruption mitigation. A tube with a cross section of $1 \text{ cm} \times 1 \text{ cm}$ and a length of 50 m can hold 35 kg of liquid tin, which is sufficient to quench runaway electrons. The ejection speed of the liquid tin is estimated to be $\sim 5 \text{ m/s}$.

8. Particle Control and Tritium Inventory

Hirooka et al. have demonstrated that when galinstan liquid is convected by the $j \times B$ force, hydrogen as well as helium particle recycling is noticeably reduced under steady state plasma bombardment [7].

The hydrogen solubility in tin is $0.47 \times 10^{-4} \text{ H/Sn}$ at 400°C and $1.54 \times 10^{-4} \text{ H/Sn}$ at 1005°C [37, 38]. This suggests that the DT particle exhaust rate with the MAGLIMD, at a tin flow rate of $2.5 \text{ m}^3/\text{s}$ at 400°C , is up to $\sim 8000 \text{ Pam}^3/\text{s}$, and that DT particles can be recovered by cooling the liquid tin.

In JET-ILW experiments, glow discharge cleaning

was performed after 200 shots of operation [39]. This result suggests that assuming an effective discharge duration of 10 s in JET experiments, steady state operation of fusion reactor that lasts much longer than 2000 s would require continuous wall conditioning; otherwise the discharge characteristics will deteriorate. The steady state particle exhaust capability of the MAGLIMD could provide continuous wall conditioning during a discharge, contributing to steady state operation.

The tritium inventory in the vacuum vessel must be controlled for safety. The tritium inventory in the MAGLIMD, with a volume of $\sim 5 \text{ m}^3$ ($2\pi \times 8.5 \text{ m} \times 0.5 \text{ m} \times 0.2 \text{ m}$), is estimated from hydrogen solubility to be 0.021 kg. This is much lower than the administrative limit of 0.64 kg for the tritium inventory in the ITER vacuum vessel [40].

9. Sputtering Yield

Enhancement of sputtering yields at elevated temperature at $\sim 400^\circ\text{C}$ was shown for lithium and tin both for deuterium and helium impact [41]. This suggests that the operating temperature could be limited due to this effect.

10. Corrosion

Corrosion of structure materials in contact with liquid metals could be problematic at high temperature. Kondo [42] showed that JLF-1 steel exposed to liquid tin at 600°C for 250 h developed a reaction layer $\sim 200 \mu\text{m}$ thick. However, corrosion of RAFM in contact with lithium can be reduced by about an order of magnitude if the temperature is reduced by 100 degrees [43], suggesting the importance of temperature control. In addition, reduction of corrosion could be possible by the proper choice of liquid metal and structural and coating materials, which are under development.

11. Summary

- 1) An innovative concept for divertor power and particle control, the magnetically guided liquid metal divertor (MAGLIMD), is proposed and discussed. This new concept could provide a simple and compact scheme for power and particle control in fusion reactors with easy maintenance and high reliability.
- 2) LM flow driven along field lines from the supply to exhaust locations will cause the entire bulk of the LM move toroidally, making the LM characteristics toroidally uniform despite the finite number of supply and exhaust points.
- 3) Tin is stable against the Rayleigh-Taylor instability during the quiescent phase of plasmas due to its high mass density, eliminating the need of a CPS to restrain its motion.
- 4) The MAGLIMD takes advantage of the LM flow along the field line oblique to the LM surface to min-

imize MHD drag. Analysis is made on the MHD drag associated with the toroidal current, driven by toroidal component of the electromotive force arising from cross-field flow. The MHD drag is expected to be acceptable and is compensated for by small steps on the LM surface and/or centrifugal force (present in the moving frame).

- 5) During the current quench in a disruption, a toroidal current is induced in the liquid metal divertor in the same direction as the plasma current. The resultant electromagnetic force pulls the main plasma toward the divertor (leading to a benign VDE), or splashes the LM toward the main plasma (providing automatic disruption mitigation).

Acknowledgments

Fruitful discussions with Prof. Y. Hirooka of Chubu Univ., Prof. K. Hanada and Prof. C. Hu of Kyushu University, Prof. T. Kunugi of Kyoto University, Dr. S. Matsuda and Prof. M. Kondo of Tokyo Institute of Technology, Dr. D.J. Campbell of ITER, Prof. Y. Ueda and Dr. T. Takizuka of Osaka Univ., Prof. T. Hino of Hokkaido Univ., Prof. A. Nishimura, Prof. J. Miyazawa and Prof. N. Noda of National Institute for Fusion Science, Drs. M. Ono, R. Kaita, M. Jaworski and R. Majeski of Princeton Plasma Physics Laboratory, Dr. G. Federici of Fusion for Energy, and research staff of National Institutes for Quantum and Radiological Science and Technology (QST) are gratefully acknowledged. The authors would like to thank Prof. N. Nakajima of International Fusion Energy Research Centre, and Drs. Y. Ikeda and Y. Sakamoto of QST for their encouragement throughout this work. This work was supported by JSPS KAKENHI Grant Number 26630475.

- [1] "Fusion Electricity: A roadmap to the realisation of fusion energy", <https://www.euro-fusion.org/wpcms/wp-content/uploads/2013/02/JG12.356-web.pdf>
- [2] The Joint-Core Team for the Establishment of Technology Bases Required for the Development of a Fusion DEMO Reactor, "Report by the Joint-Core Team for the Establishment of Technology Bases Required for the Development of a Fusion DEMO Reactor", Jan. 2015, http://www.jspf.or.jp/2015/genkeiro/150119_v6.pdf
- [3] R.A. Pitts *et al.*, *J. Nucl. Mater.* **438**, S48 (2013).
- [4] Y. Sakamoto *et al.*, IAEA FEC (2014) FIP/3-4Rb.
- [5] Y. Ueda *et al.*, *Nucl. Fusion* **57**, 092006 (2017).
- [6] M. Shimada and Y. Hirooka, *Nucl. Fusion* **54**, 122002 (2014), <https://doi.org/10.1088/0029-5515/54/12/122002>
- [7] Y. Hirooka *et al.*, *Fusion Eng. Des.* **117**, 140 (2017), <http://dx.doi.org/10.1016/j.fusengdes.2016.06.028>
- [8] J. Miyazawa *et al.*, *Fusion Eng. Des.* **125**, 227 (2017).
- [9] K. Tobita *et al.*, *Nucl. Fusion* **49**, 075029 (2009), <https://doi.org/10.1088/0029-5515/49/7/075029>
- [10] Shercliff, *Proc. Cambridge Philosophical Society* **49** (1953) pp.136-144.
- [11] L. Battezzati, *Acta Metall.* **37**, 1791 (1989).
- [12] Y. Gribov *et al.*, *Nucl. Fusion* **47**, S385 (2007).
- [13] A. Hassanein, *Atomic and Plasma-Material Interaction Data for Fusion (Supplement to the journal Nuclear Fusion)* **5**, 193 (1994).
- [14] M.A. Jaworski *et al.*, *J. Nucl. Mater.* **415**, S985 (2011).
- [15] P. Fifiis *et al.*, *Nucl. Fusion* **56**, 106020 (2016).
- [16] A.V. Chankin, *J. Nucl. Mater.* **196-198**, 739 (1992).
- [17] K. Itami, *Proc. 14th Int. Conf. Plasma Physics and Controlled Nuclear Fusion Research (Würzburg) IAEA-CN-56/A-6-5*.
- [18] A. Kumagai *et al.*, *Plasma Phys. Control. Fusion* **39**, 1189 (1997).
- [19] J.V. Lingertat, *J. Nucl. Mater.* **241-243**, 402 (1997).
- [20] R.A. Pitts, *Nucl. Fusion* **43**, 1145 (2003).
- [21] T. Eich, *J. Nucl. Mater.* **363-365**, 989 (2007).
- [22] R.A. Pitts, *Nucl. Fusion* **47**, 1437 (2007).
- [23] M.A. Jaworski, *Plasma Phys. Control. Fusion* **55**, 124040 (2013).
- [24] P. Harbour, *Contrib. Plasma Phys.* **28** (4/5), 417 (1988).
- [25] P.J. Harbour, *J. Nucl. Mater.* **162-164**, 236 (1988).
- [26] A.V. Chankin, *J. Nucl. Mater.* **196-198**, 739 (1992).
- [27] B.B. Alchagirov *et al.*, *High Temperature* **47**, 287 (2009).
- [28] J.A. Cahill, *J. Inorg. Nucl. Chem.* **26**, 206 (1964).
- [29] J. Li *et al.*, *Trans. Nonferrous Met. Soc. China* **15**, 1166 (2005).
- [30] V.A. Evtikhin *et al.*, *J. Nucl. Mater.* **271&272**, 396 (1999).
- [31] A.V. Chankin, *Plasma Phys. Control. Fusion* **56**, 025003 (2014).
- [32] R. Dux, *Nucl. Fusion* **51**, 053002 (2011).
- [33] M.J. Higgins *et al.*, *Atomic and Molecular Data for Fusion, Part 3, "Recommended Cross Sections and Rates for Electron Ionization of Atoms and Ions: Copper to Uranium"*. Culham Laboratory, Report CLM-R294 (1989).
- [34] J.W. Coenen *et al.*, *Nucl. Fusion* **51**, 083008 (2011).
- [35] K. Krieger, *J. Nucl. Mater.* **415**, S297 (2011).
- [36] G. Miloshevsky and A. Hassanein, *Nucl. Fusion* **54**, 043016 (2014).
- [37] K. Iwase, *Sci. Rep. Tohoku Univ., First Ser.* **15** (1926) p.531.
- [38] R.A. Causey, *J. Nucl. Mater.* **300**, 91 (2002).
- [39] D. Douai *et al.*, *J. Nucl. Mater.* **438**, S1172 (2013).
- [40] M. Shimada and R.A. Pitts, *J. Nucl. Mater.* **415**, S1013 (2011).
- [41] J.P. Allain, "Kinematic and Thermodynamic Effects on Liquid Lithium Sputtering," Ph.D. Thesis, NPPE, University of Illinois, Champaign-Urbana, 2001.
- [42] M. Kondo *et al.*, *Fusion Eng. Des.* **98-99**, 2003 (2015), <http://dx.doi.org/10.1016/j.fusengdes.2015.05.051>
- [43] T. Muroga *et al.*, IAEA FEC (2008) FT/4-3Rb, http://www-pub.iaea.org/MTCD/Meetings/FEC2008/ft_4-3rb.pdf